Applied Energy 336 (2023) 120853

Contents lists available at ScienceDirect

Applied Energy

journal homepage: www.elsevier.com/locate/apenergy

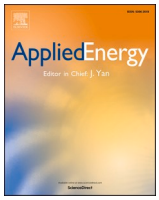

Interfacial engineering via laser ablation for high-performing PEM water electrolysis

Jason K. Lee [a], Tobias Schuler [b], Guido Bender [b], Mayank Sabharwal [a], Xiong Peng [a,*], Adam Z. Weber [a], Nemanja Danilovic [a,*]

[a] Energy Storage and Distributed Resources Division, Lawrence Berkeley National Laboratory, Berkeley, CA 94720, United States of America
[b] Chemistry and Nanoscience Center, National Renewable Energy Laboratory (NREL), Golden, CO 80401, United States

HIGHLIGHTS

- Laser ablation alters titanium at the interface, forming more uniform structure like a microporous layer or backing layer.
- Laser ablation is a facile method for mass production compared to other fabrication methods for creating a backing layer.
- Our PEMWEs exceed reported performance at 80 °C, using commercial materials at lowest loadings reported at 0.05 mg_{Ir}/cm^2.
- Bulk modification of the PTL improves mass transport without sacrificing interface.

GRAPHICAL ABSTRACT

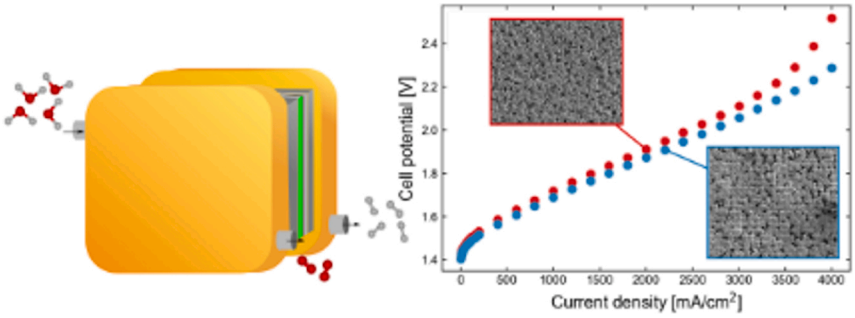

ARTICLE INFO

Keywords:
Water electrolysis
Proton exchange membrane
Porous transport layer
Interface
Laser ablation

ABSTRACT

A rationalized interfacial design strategy was applied to tailor the porous transport layer (PTL)-catalyst layer (CL) contact and the PTL bulk-phase architecture. Particularly, at the PTL-CL interface, our results reveal that laser ablated sintered titanium power-based PTLs improve electrolyzer performance at both the H2NEW Consortium baseline catalyst loading of 0.4 $mg_{Ir}\cdot cm^{-2}$ as well as at the ultra-low catalyst loading of 0.055 $mg_{Ir}\cdot cm^{-2}$. Under ultra-low catalyst loadings, the laser ablated PTL demonstrates maximum reduction of 230 mV compared to the commercial PTL at 4 $A\cdot cm^{-2}$, and reduces by 68 mV at 3.2 $A\cdot cm^{-2}$ under H2NEW baseline loading. Laser ablation alters the titanium phase at the interface, so it forms more uniform structure like a microporous layer or a backing layer, leading to an increase in the surface area in contact with the catalyst layer while preventing the membrane from deforming into the PTL. Moreover, we reveal that bulk-phase architecture modification of the PTL by ablating patterned pores at the flow field-PTL interface improves mass transport without sacrificing contact at the CL-PTL interface. Overall, laser ablation of the PTL is an effective method to customize interfacial design to enhance proton exchange membrane electrolyzer performance.

* Corresponding authors.
E-mail addresses: xiongp@lbl.gov (X. Peng), ndanilovic@lbl.gov (N. Danilovic).

https://doi.org/10.1016/j.apenergy.2023.120853
Received 9 August 2022; Received in revised form 25 January 2023; Accepted 13 February 2023
Available online 28 February 2023

1. Introduction

With global CO_2 emissions rebounding to peak again after a short decline from pandemic, demands for electrification of energy related sectors have escalated to curtail anthropogenic emissions [1]. The challenge in decarbonization of energy related sectors arises from heavy dependence on fossil fuels for diverse applications such as in power, transportation, industry, and district heating [2,3]. However, decarbonization of these sectors cannot solely be realized through electricity. Hydrogen is an excellent alternative to fossil fuels that can power various sectors including the power sector [4], heavy-duty transportation sector [5], district heating sector [6], and extending on to industrial sectors to be used as chemical feedstock to produce ammonia [7] or metals [8]. Currently, approximately 95% of hydrogen produced today are gray hydrogen, which comes from reforming hydrocarbons and leaves immense carbon footprint during hydrogen production [9]. Therefore, continuously relying on gray hydrogen demeans the purpose of shifting towards alternative fuels. On the other hand, green hydrogen, which is hydrogen produced via electrolysis powered by renewables, leaves no carbon footprint and thus is a key that complements the usage of renewables while shifting towards green hydrogen economy [10].

Proton exchange membrane (PEM) water electrolyzer is one of the most promising electrolysis techniques for green hydrogen production. When powered by renewables, a PEM electrolyzer cell converts liquid water into hydrogen and oxygen gases in the absence of carbon emissions. Hence, PEM electrolyzers carry enormous potential in leveraging a shift from gray hydrogen to green hydrogen at the heart of energy related sectors. To achieve this shift towards green hydrogen, cost reduction of PEM electrolyzer technology is inevitable. With increasing supply of renewables curtailing the cost of electricity [11], the next task in PEM electrolyzer research is to reduce capital expenditures especially at larger production scales. This requires minimizing voltage losses occurring at higher current densities while significantly reducing precious metal catalyst loadings. Specifically, since the amount of precious materials required in the electrolyzer is predicted to increase substantially at a GW scale [12], there needs to improve and optimize electrolyzer components so it exhibits low cell potential at lower catalyst loadings.

The interplay of a porous transport layer (PTL) in providing a firm contact at the catalyst layer and facilitating effective mass transport and charge transfer is a critical design consideration in the PEM electrolyzer system. The titanium phase in contact with anode catalysts completes a pathway for electrons to transfer to reaction sites. Previous studies emphasize that the contact between the PTL and the catalyst layer significantly impacts the electrolyzer performance, where highly porous interface reduces the electron conductivity thereby lowering catalyst utilization [13–15]. Conversely, dense catalyst layer and PTL interface (CL-PTL interface) increases mass transport losses from accumulation of gases over the reaction surface, limiting the transport of liquid water to the reaction surface [16]. Taie et al. have demonstrated that these interfacial impacts on electrolyzer performance intensifies under ultra-low catalyst loadings because the number of reaction sites decreases [17]. Rationally modified PTLs have been proven to improve electrolyzer performance from enhanced interfacial properties. For instance, PTLs with porosity gradient (or PTLs with a backing layer) fabricated via vacuum plasma spraying exhibited improved contact and mass transport, extending the performance of electrolyzers [18–21]. A microporous layer (MPL) has been constructed on the PTL by Schuler et al. [22], where they observed increased catalyst utilization by a factor of 2.2 and reduction of mass transport losses by 45%. PTLs with patterned structure have also shown to improve performance of the electrolyzer, where the perforated pores in the PTL enable effective bubble detachment, enhancing the mass transport during electrolysis [23–26]. Moreover, previous studies have attempted in modifying microstructure of the PTL to improve the electrolyzer performance [27,28]. Specifically, Suermann et al. [27] have demonstrated improved ohmic and mass transport performance of felt-based PTLs by using femtosecond laser to modify microstructure of the felt material. Femtosecond laser provides a small pulse width with a high peak power, which results in a small heat influence zone that can be used to alter microstructure of each individual fiber in the felt PTL. These previous studies direct that novel rationalized PTL designs are necessary for improving performance of the electrolyzer and ultimately curtail the cost of green hydrogen.

In this study, we present novel PTL designs fabricated by applying laser ablation to a commercially available sintered titanium powder-based PTL. Laser ablation offers an effective method for rationally customizing macrostructure at the CL-PTL interface, providing similar advantages as PTLs with an MPL or a backing layer. Tailoring laser ablation pathways and path spacing (d_{path}) (Fig. 1) have resulted in two distinct interfacial patterns at the CL-PTL interface: a parallel pattern and a cross pattern. Surface morphology of these interfacial patterns are first characterized by observing at the PTL surface as well as the anode side of the CCM post to the electrolyzer operation. Then, the impact of laser ablation patterns on the performance of the electrolyzer under ultra-low catalyst loadings is evaluated through various electrochemical techniques. Lastly, the effect of the laser ablated PTLs at high catalyst loading conditions has been investigated, along with the impact of laser ablation on the bulk structure of PTL. Our results demonstrate the feasibility of laser ablation to customize PTL interfacial design and the effectiveness of improving PEMWE performance.

2. Results

2.1. Laser ablated porous transport layers

Controlling laser ablation pathways and d_{path} results in two distinct patterns at the CL-PTL interface as seen in Fig. 2. Laser ablation in parallel patterns imprint land-channel structure on the PTL (Fig. 2a-d), and laser ablation in cross patterns inscribe checker-like structure on the PTL (Fig. 2e-h). The PTL surface affected by the laser becomes smooth while the surface unaffected by the laser, such as the land region in Fig. 2b and c, maintains original roughness. Controlling d_{path} dictates the exposure of the PTL surface to laser ablation, and a large change in d_{path} results in a completely different PTL morphology albeit undergoing the identical laser ablation pathway as seen in Fig. 2 (higher magnification images seen in Fig. S1).

Ablating laser in parallel paths forms land-channel structure at the CL-PTL interface. Specifically, laser ablation smooths out the channel region (Fig. S1), providing enhanced connectivity to the pores in the PTL, which facilitates the gas removal process. Also, the land structure increases interfacial surface contact area between the PTL and the catalyst layer. Widths of the land region increases when d_{path} is increased, where the PTL with d_{path} = 127 μm exhibits largest land features and the PTL with d_{path} = 38 μm barely shows land-channel structure. Since overall number of laser paths increase with shorter d_{path}, the PTL with d_{path} = 38 μm obtains more of a granular structure from laser melting titanium powders on the surface, which further reduces the surface roughness of the PTL. Compared to the pristine PTL (Fig. S1g), the pores in parallel patterned PTLs show higher connectivity.

In cross patterned PTLs, laser ablation imprints checker-like structure. Longer d_{path} decreases surface roughness of the PTL and flattens out the PTL interface. In particular, higher magnified SEM image shown in Fig. S1f shows that the cross pattern PTL with d_{path} = 127 μm effectively melts the titanium particles resulting in closure of many surface pores at the PTL interface, which can effectively enhance the contact with the catalyst layer. This structure also minimizes membrane deformation into the PTL interface and prevent the catalyst layer deformation within the large pores of conventional PTL structures, which decreases electrical and ionic conductivity within the catalyst layer as previously reported by Schuler et al. [13,14] Membrane deformation could also lead to local membrane thinning, therefore leaching fluoride ion, which in return

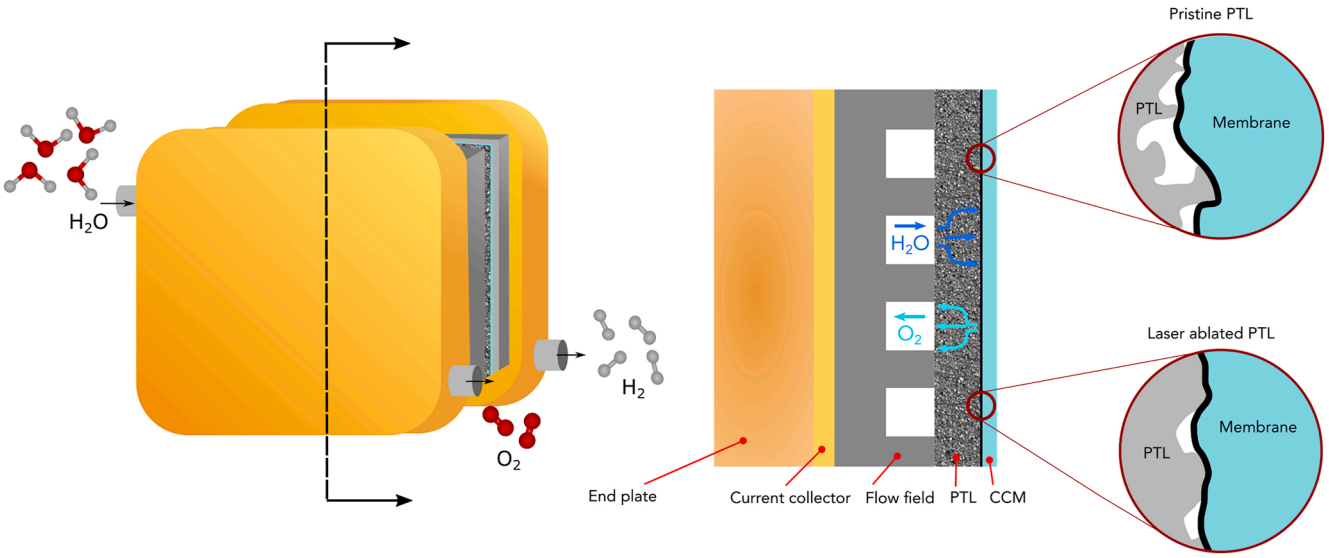

Fig. 1. The schematic of the laser ablation patterns on the catalyst layer-PTL interface.

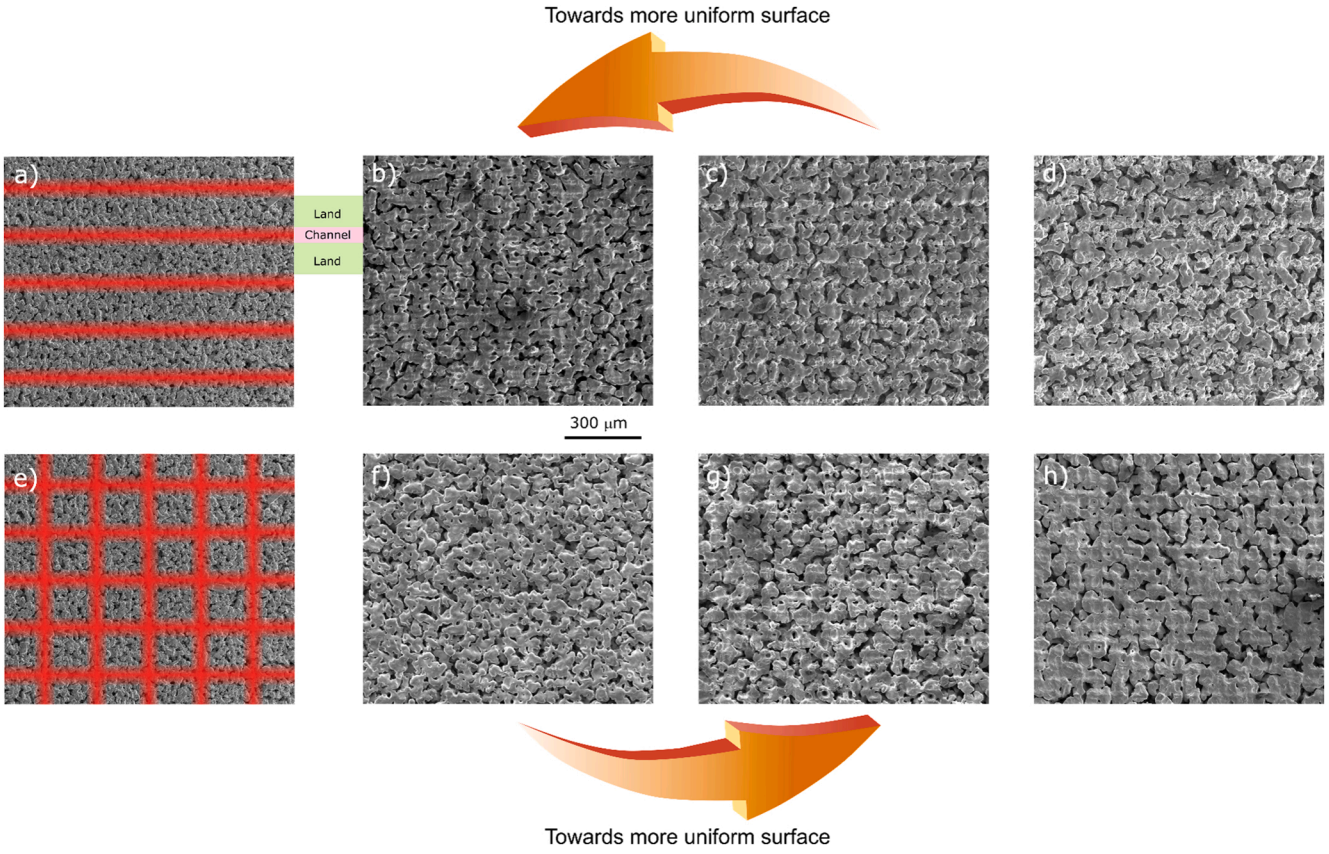

Fig. 2. SEM images of the laser ablated sintered titanium-based PTLs. Schematics of laser paths for parallel and cross patterns are as shown in (a) and (e), respectively. Parallel patterns with d_{path} = (b) 38 μm, (c) 76 μm, and (d) 127 μm. Wider d_{path} imprints more evident land-channel structure at the CL-PTL interface. Cross patterns with d_{path} = (f) 38 μm, (g) 76 μm, and (h) 127 μm. Wider d_{path} results in more concise checker-like structure at the CL-PTL interface. Laser ablation closes some of the surface pores with the cross paths with $d_{path} > 76$ μm. For parallel patterns, smaller d_{path} results in more uniform surface while for cross patterns, larger d_{path} results in more uniform surface.

exacerbates electrolyzer component degradation. When d_{path} decreases, surface roughness increases and the interface gains more granular structure. Specifically, increased number of laser paths from having shorter d_{path} over melt the PTL interface causing formation of tiny pores within titanium phase that appear to be dead-ended (Fig. S1d). Dead-ended pores block transport of both liquid water and oxygen gas, which causes loss of effective interfacial contact between PTL and CL.

The interfacial contact area of the catalyst layer and PTL has been further analyzed through synchrotron X-ray computed tomography (XCT) obtained from the Advanced Light Source at Lawrence Berkeley

National Laboratory (Beam-line 8.3.2). The tomographic images acquired for a pristine PTL, and a laser ablated PTL (cross patterned PTL with 127 μm spacing) are as shown in Fig. 3. The XCT image of the laser ablated PTL (subset of Fig. 3) exhibits flat and planar surface created by heat from the laser, and this leads to enhanced interfacial contact area against the catalyst layer compared to the baseline PTL. Similar observations on interfacial contact have been made via SEM image processing (Fig. S3, Fig. S4) and optical profilometer (Fig. S6), where laser ablated regions improve the point of contact with the catalyst layer. The surface analysis directs that laser ablation is a promising yet facile process for modifying the PTL interfacial structure for improving performance of PEM water electrolzyers.

2.2. Impact of laser ablation patterns on electrochemical performance under ultra-low Ir loading conditions

2.2.1. Parallel patterned porous transport layer with Land-Channel structure

Electrochemical performance of electrolyzers assembled with parallel patterned PTLs under the ultra-low catalyst loading condition (0.055 mgIr·cm^{-2}) is shown in Fig. 4. All parallel patterned PTLs with 3 different d_{paths} (38 μm, 76 μm, 127 μm) outperform the baseline PTL up to current density of 2.8 A·cm^{-2}. Above 2.8 A·cm^{-2}, overpotentials for the PTL with d_{path} = 127 μm start to increase, eventually exceeding the overpotential of the baseline PTL at 3.2 A·cm^{-2}. The parallel patterned PTLs with d_{path} = 38 μm and 76 μm outperform the baseline PTL throughout the tested current density. The PTL with smallest path spacing exhibits lowest cell potential.

Parallel patterns at the CL-PTL interface fabricated through laser ablation improve kinetic performance during water electrolysis. All three parallel patterned PTLs experience lower kinetic overpotential compared to the baseline PTL as shown in Fig. 4b, and the PTL with the smallest d_{path} exhibit the lowest kinetic overpotential (30 mV improvement against baseline). This improvement in kinetics stems from the improved contact at the CL-PTL interface, which improves charges transfer as also observed with smaller Tafel slope (discussion below). It's also worth noting that PTLs with distinct land-channel structure at the CL-PTL interface (d_{path} = 76 μm and 127 μm) has less improvement on the kinetics probably due to impacted electrical conductivity within the catalyst layer caused by the membrane deforming into the channel region of the PTL. Catalyst layer deformation can impact catalyst utilization by impacting catalyst electrical conductivity especially at low loadings [13,14,17].

Land-channel structure in the parallel patterned laser ablated PTL (Fig. 2 c, d) reduces the high frequency resistance (HFR). Fig. 4c shows PTLs with d_{path} = 76 μm and 127 μm displaying lower HFRs in contrast to the other two PTLs. When the land-channel structure exists at the CL-PTL interface, local over-compression can squeeze the membrane, which reduces the effective proton transport distance between anode and cathode, therefore leading to lower measured HFR compared to the baseline PTL. At higher current densities, HFRs start to increase, where the rate of HFR increase becomes more prominent for d_{path} = 127 μm, which has more protuberant land-channel structure. This increase in HFR is associated with the gas accumulation in channel regions of the CL-PTL interface. Higher gas content accumulates at high current densities in the channel region of the CL-PTL interface, thereby dehydrating membrane with increased HFR. Moreover, this increase in HFR is observed with the increase in the mass transport losses. The build-up of gas exacerbates mass transport losses in these laser ablated PTLs with land-channel structure (Fig. 4d). PTLs with wider channel regions suffer more from increased mass transport as observed by higher mass transport overpotential for d_{path} = 127 μm compared to d_{path} = 76 μm. It can be seen that the channel region of the pattern behaves similar to delamination at the CL-PTL interface leading to accumulation of gas, as reported previously [29]. Of the tested parallel patterned PTLs, the PTL with d_{path} = 38 μm, which has granular structure than land-channel structure (Fig. S1a-c), demonstrates the best cell performance.

2.2.2. Cross patterned porous transport layer with checker-like structure

Applied voltage breakdown of electrolyzer performance operating with cross patterned PTLs under the ultra-low catalyst loading is shown in Fig. 5. Except for the PTL with d_{path} = 38 μm, which experience significant overpotentials at current densities >2.0 A·cm^{-2}, cross patterned PTLs outperform the baseline PTL. Unlike the trend observed for parallel

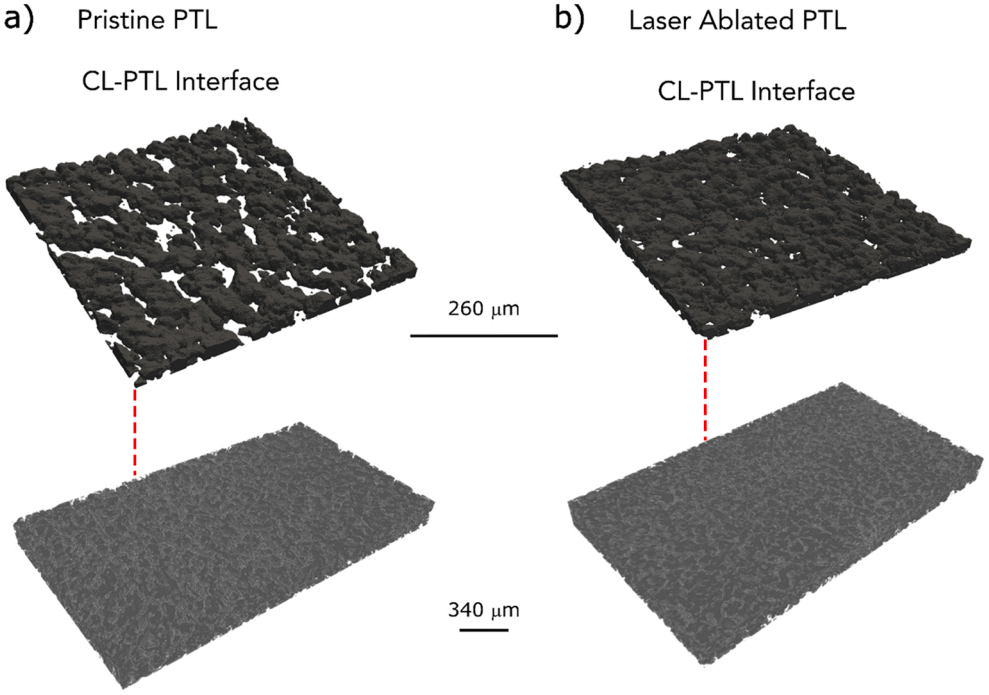

Fig. 3. X-ray computed tomographic images of (a) a pristine PTL and (b) a laser ablated PTL. The CL-PTL interface of the two PTLs is shown as a subset figure. The laser ablated morphology provides enlarged contact surface between the PTL and CL.

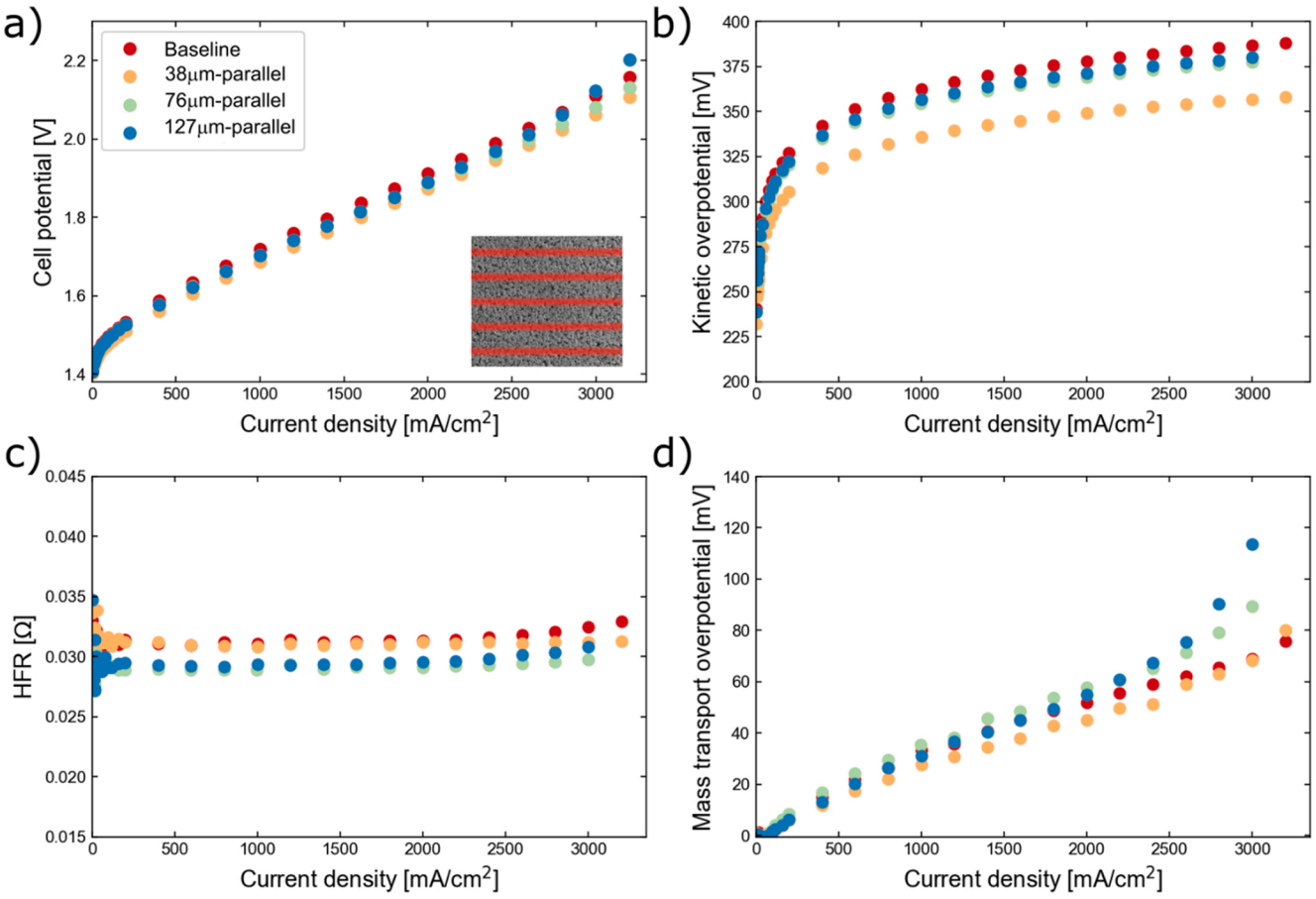

Fig. 4. Applied voltage breakdown of laser ablated PTLs with land-channel structure. (a) Polarization curve, (b) kinetic overpotential, (c) high frequency resistance and (d) mass transport overpotential in comparison to the baseline PTL at ultra-low loading (0.055 mg·cm^{-2}). While HFR and kinetic improves with land-channel pattern at the CL-PTL interface, mass transport losses emanate from accumulation of the gas at the channel region. Larger d_{path} leads to higher mass transport overpotential.

patterned PTLs, cross patterned PTLs improve electrolyzer performance with increasing d_{path}. This is because laser ablation in a cross-pattern provides more uniform modification at the interface rather than concentrating at the specific regions as parallel passes do. In addition, increasing d_{path} avoid overmelting the titanium interface for cross patterns since higher number of d_{path} reduces the total number of laser ablation passes.

Cross patterns imprint checker-like structure at the CL-PTL interface, and wider d_{path} further reduces surface roughness of the PTL. Laser ablation in a cross pattern deforms titanium particles and flattens out the titanium phase at the interface. As titanium particles melt during laser ablation, they fill-in smaller surface pores with titanium phase, increasing surface area at the CL-PTL interface. The shallow deformation of the membrane observed at $d_{path} = 127$ μm is evidence that deformed titanium particles enhance the interfacial contact, which will be discussed later. Improve kinetic performance of the electrolyzer under low loading conditions is seen in Fig. 5b, where the cross patterned PTL with widest d_{path} exhibits lowest kinetic overpotential. Furthermore, checker-like structure reduces HFR of the electrolyzer. In particular, PTLs with $d_{path} = 76$ μm and 127 μm exhibit the lowest HFR. Instead of the local compression effect as observed in parallel patterned PTLs, the cross patterned laser ablated PTLs' flattened morphology (seen from surface profiles in Fig. S6) increases the interfacial contact area while prohibiting intrusion of membrane into the interfacial pores at the PTL. Therefore, the catalyst layer maintains firm contact, preventing the spread of iridium particles and preserving electrical conductivity within the catalyst layer [13,14]. This effect is even more sensitive under ultra-low loading conditions as the content of iridium oxide in the catalyst layer is significantly reduced under low loading conditions. Hence, the HFR values remain constant throughout current densities (Fig. 5c), while HFR values of parallel patterned PTLs increase at high current densities. Cross patterned PTLs with $d_{path} = 76$ μm and 127 μm provide similar advantages as that of an MPL or a backing layer, which enhances the contact against the catalyst layer. In contrast, the cross patterned PTL with $d_{path} = 38$ μm forms agglomerate structure from over-melting titanium particles, which creates small dead-ended pores at the interface as a by-product.

Fig. 5d shows that the checker-like structure of laser ablated PTLs increases mass transport overpotentials at higher current densities under ultra-low loading conditions. Since the catalyst layer is significantly thinner and denser under low loading [17], mass transport occurring within the catalyst layer (i.e., in-plane direction) becomes less significant, and mass transport would mostly occur through pores at the CL-PTL interface (i.e., through-plane). As fewer pore openings are available for mass transport at the interface of cross patterned PTLs (Fig. 2 and Fig. 3), these PTLs exhibit slightly higher mass transport overpotentials compared to the baseline PTL (16 mV at 3.2 A·cm^{-2}). Nevertheless, improvements in the high frequency resistance and kinetics overcome increased mass transport overpotentials when using electrolyzers operating with cross patterned PTLs.

The best performing laser ablated PTL, which is the cross patterned PTL with $d_{path} = 127$ μm, and the baseline PTL has been operated up to 4 A·cm^{-2} to investigate the impact of PTL interface on higher current density operations (Fig. S5). A surprising cell potential reduction of 230 mV has been achieved at 4 A·cm^{-2} between the laser ablated PTL and the baseline PTL. Our laser ablated PTL exhibits similar or even

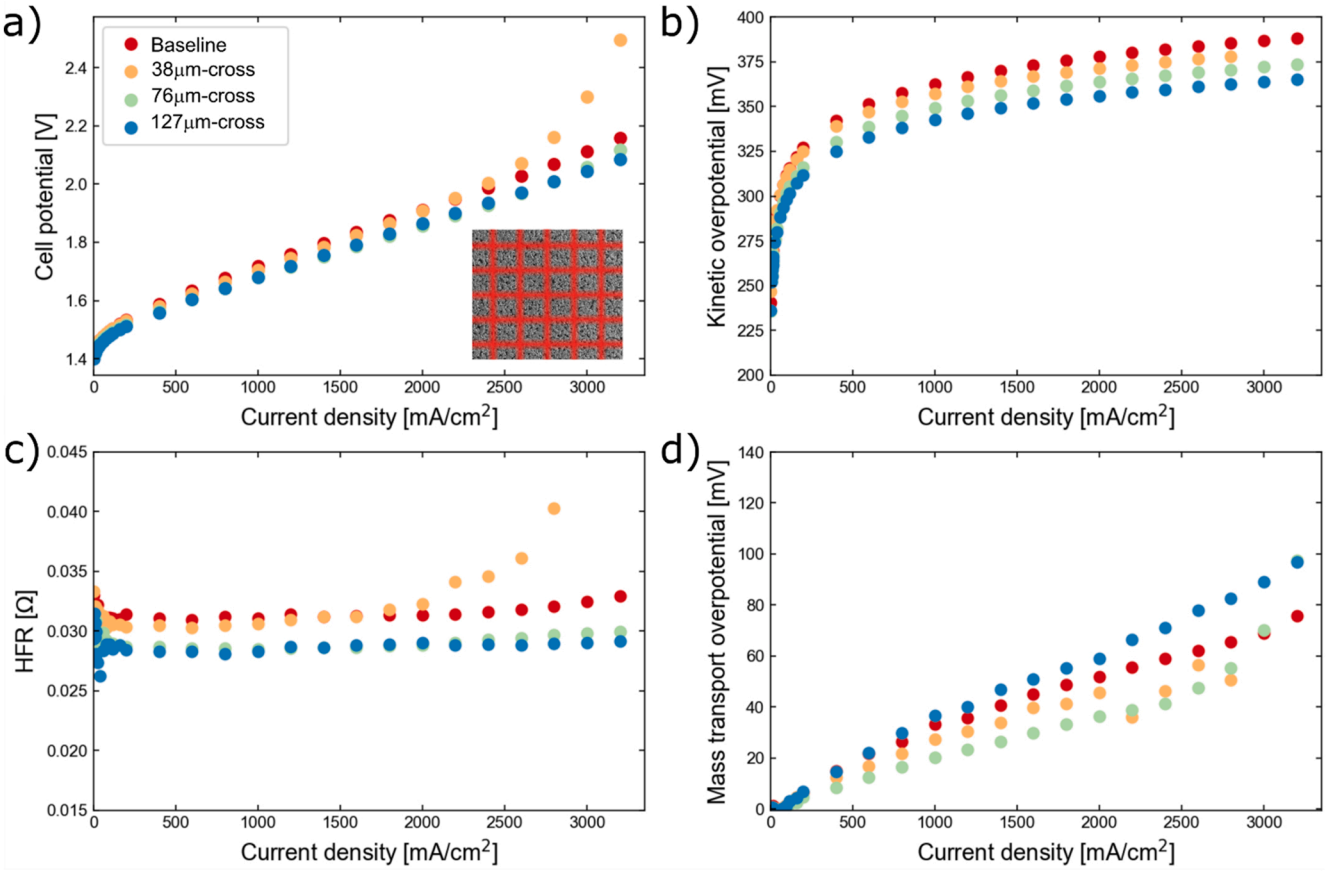

Fig. 5. Applied voltage breakdown of laser ablated PTLs with checker-like structure. (a) Polarization curve, (b) kinetic overpotential, (c) high frequency resistance and (d) mass transport overpotential in comparison to the baseline PTL at ultra-low loading (0.055 mg·cm^{-2}). Checker-like structure at the CL-PTL interface improves both HFR and kinetic performance. Increasing d_{path} further improves HFR and kinetics. Slightly higher mass transport overpotential observed for 127 μm however is significantly lower than land-channel structured PTLs.

improved performance compared to bi-layer structured PTLs reported in literature although we use thicker membrane (~50 μm thicker) at ultra-low iridium loading (reduction greater than ×40) [18,19,21,22]. Under ultra-low loading and high current density operation, the baseline PTL experiences increase in HFR and mass transport from accumulation of gas at the interface reducing the electrochemical surface area from dehydrating the membrane and thereby decreasing the catalyst utilization. In contrast, the laser ablated PTL preserves the electrochemical surface area even at higher current densities and hence maintains catalyst utilization. In addition, the laser ablated PTL minimizes the accumulation of gas, dampening the increase in mass transport overpotentials ($i > 3.5$ A·cm^{-2}). Our work demonstrates that laser ablation is an effect approach to improve electrolyzer performance under ultra-low catalyst loadings.

2.2.3. Impact of PTL-CL interfacial engineering on electrode kinetics

Tafel and EIS analysis provide another insight on how laser ablation improves water electrolyzer performance. Fig. 6a shows an overlay of Tafel slopes on measured cell potentials at ultra-low loading for baseline and parallel patterned PTLs. All modified PTLs exhibit lower Tafel slope compared to the baseline (Table 1), with 38 μm d_{path} experiencing lowest value of the Tafel slope. This observation is in agreement with the EIS results shown in the Nyquist plot measured at 1 A·cm^{-2} for the parallel patterned PTLs in Fig. 6c. All Nyquist plots show a single semicircle loop, indicating the anode oxygen evolution reaction dominates the electrode behavior at this current. The difference between two intercepts at high and low frequency regions indicates a lower charge transfer resistance for laser ablated PTLs, with d_{path} = 38 μm the lowest, suggesting improved electrode kinetics compared to baseline PTL.

The Tafel slope measured from cross patterned PTLs are shown in Fig. 6b. Laser ablated PTLs exhibit improved Tafel kinetics compared to the baseline. The smoothened surface from the laser ablation improves contact at the CL-PTL interface, not only improving kinetics but also reducing HFR under ultra-low catalyst loading conditions. The corresponding Nyquist plot (Fig. 6d) shows that for d_{path} = 76 μm and 127 μm, laser ablated PTLs significantly reduce HFR, which is similar to the case for parallel patterned PTLs. Overall, the Tafel slopes (Table 1) and Nyquist plots suggest that laser ablation can not only alter the ohmic resistance but also improves electrode kinetics during electrolysis, indicating that both the contact resistance and reaction charge transfer resistance can be impacted by interfacial contact between PTL and CL.

2.2.4. Impact of laser ablated PTLs on catalyst coated membrane post to operation

Observing the anode side of CCMs post to the electrolyzer operation enables more in-depth analysis of the PTL-CL interface of laser ablated PTLs (Fig. 7). Parallel patterned PTLs with d_{path} = 76 μm and 127 μm, which clearly portrays land-channel structure at the PTL interface, imprint land-channel structure in the membrane as well. These land-channel structures are formed by membrane deformation caused by high compression from PTL's land region, which forces the membrane to deform towards the channel region. The parallel patterned PTL with larger d_{path} shows more notable land-channel structure. This land-channel structured deformation is less favorable for electrolyzer performance because the deformation of membrane into the channel region decreases electronic conductivity in the catalyst layer as mentioned by Schuler et al. [13,14], which also reduces catalytic utilization, leading to increase of electrode kinetic overpotential in Fig. 4b. Moreover, the

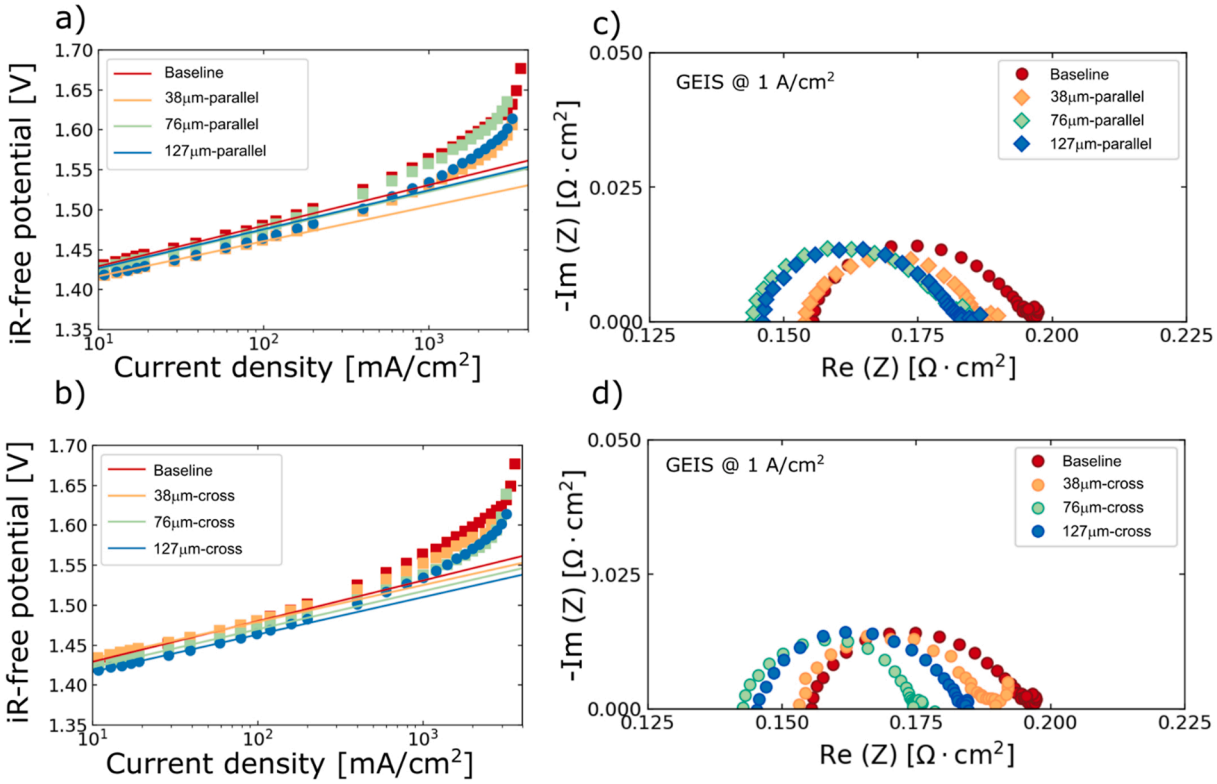

Fig. 6. Tafel analysis for (a) parallel patterned PTLs and (b) cross patterned PTLs. Galvanostatic electrochemical impedance spectroscopy measurement at 1 A·cm^2 for (c) parallel patterned PTLs and (d) cross patterned PTLs.

Table 1
Tafel slopes for baseline and laser ablated PTLs.

Sample	Tafel Slope [mV/dec]
Baseline	50.8
38 μm Parallel	43.7
76 μm Parallel	48.4
127 μm Parallel	48.9
38 μm Cross	46.1
76 μm Cross	47.6
127 μm Cross	46.7

channel region at the PTL-CL interface acts as delamination, further exacerbating the interfacial contact while also accumulating the delaminated space with gas, germinating significant mass transport losses. As a result, increases in HFR as well as mass transport losses are observed with PTLs featuring land-channel structure (Fig. 4c, d). The parallel patterned PTL with d_{path} = 38 μm imparts granular structure rather than land-channel structure since the PTL itself has more of a granular structure. As a result, the post operation image shows smoother CCM surface.

Cross patterned PTLs also impart granular structure (Fig. 2a, d-f) on the membrane when assembled in the electrolyzer (Fig. 7, higher magnification images in Fig. S2). Compared to deformation observed in the baseline PTL (Fig. 7g), deformation from checker-like structure of cross patterned PTLs portrays larger granular structure, resulted from being compressed by molten titanium agglomerates at the PTL interface. When a laser ablates the PTL surface in a cross pattern, it melts and merges titanium particles together forming larger titanium agglomerates (Fig. 2f). Moreover, laser ablated surfaces show lower surface roughness compared to the baseline PTL, which improves the interfacial contact at the CL-PTL interface. A CCM assembled with the cross pattern PTL with d_{path} = 127 μm imparts most uniform deformation amongst tested PTLs (Fig. 7f), which is in agreement with the electrochemical performance test where this PTL demonstrated superior performance amongst other tested PTLs. The laser ablation of the PTL surface enhances the contact at the catalyst layer in a similar mechanism as to a backing layer or an MPL. However, laser ablation removes material from the PTL reducing the thickness whereas application of backing layers or MPLs adds on extra PTL thickness, increasing tortuosity and possibly exacerbating mass transport properties at higher current densities [22,30,31].

2.2.5. *Cross patterned porous transport layer at high loading conditions*

The performance improvement achieved with the cross patterned PTL under high catalyst loading conditions (0.40 mg·cm^{-2}, which is the baseline loading for H2NEW consortium) is shown in Fig. 8. The cross patterned PTL (d_{path} = 127 μm) demonstrates lower cell potential than the baseline PTL under the high catalyst loading condition. The laser ablated PTL reaches just below 2 V at 3.2 A·cm^{-2}, while the baseline PTL reaches about 2.07 V at the same current density. The main contributors to performance improvements are attributed to the lower HFR and mass transport overpotential. Two PTLs exhibit nearly identical kinetic performance. This is likely due to the electrode kinetics dictated by catalyst loading rather than the PTL-CL interfaces.

Checker-like structure provides firm contact at the CL-PTL interface. As a result, reduction in the HFR is observed even under higher catalyst loadings when the laser ablated PTL is used. The d_{path} = 127 μm cross patterned PTL used for the high loading test provides enlarged interfacial contact surface against the catalyst layer, which minimizes membrane intrusion into the PTL; therefore, prohibiting membrane deformation into the PTL and preventing loss of electrical conductivity within the catalyst layer even at higher loading conditions. Yet, kinetic performance remains fairly similar to the baseline PTL because sufficient reaction sites are available under higher loading conditions in contrast to low loading conditions.

Furthermore, checker-like structure in the PTL improves mass transport under high catalyst loadings, which is different from the trend

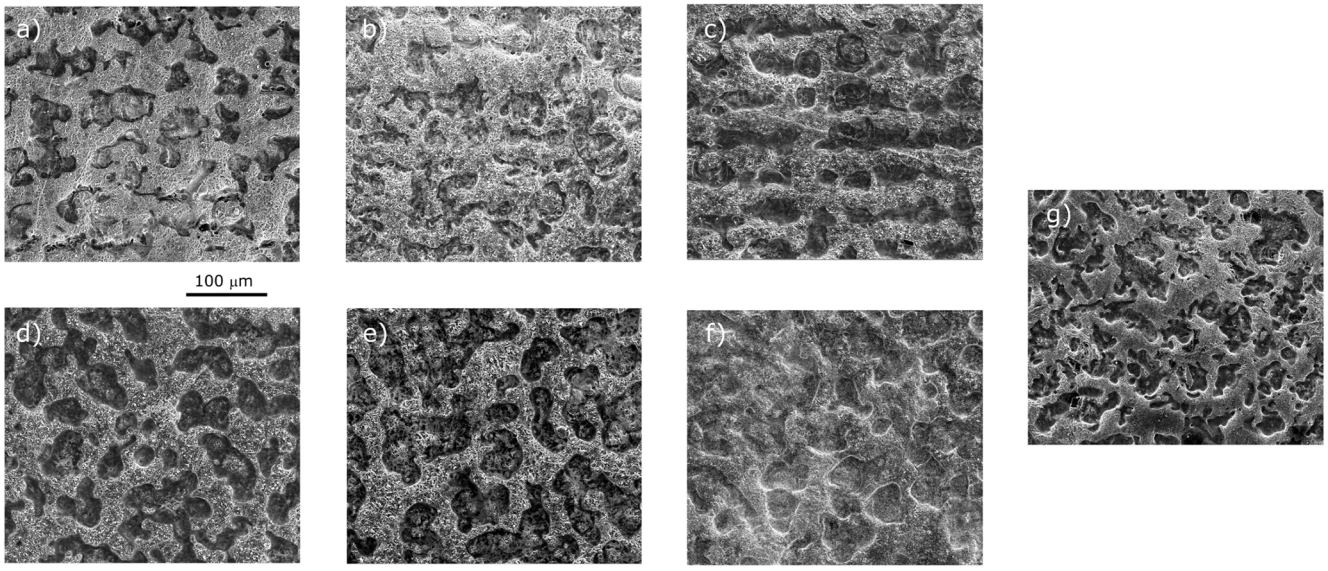

Fig. 7. SEM images of CCMs post to the electrolyzer operation. Parallel patterns with d_{path} = (a) 38 μm, (b) 76 μm, and (c) 127 μm. Wider d_{path} results in more distinct imprints of the land-channel structure on the CCM. Cross patterns with d_{path} = (d) 38 μm, (e) 76 μm, and (f) 127 μm. Wider d_{path} results in more uniform CL-PTL interface. (g) An SEM image of the CCM post to the electrolyzer operation with the baseline PTL.

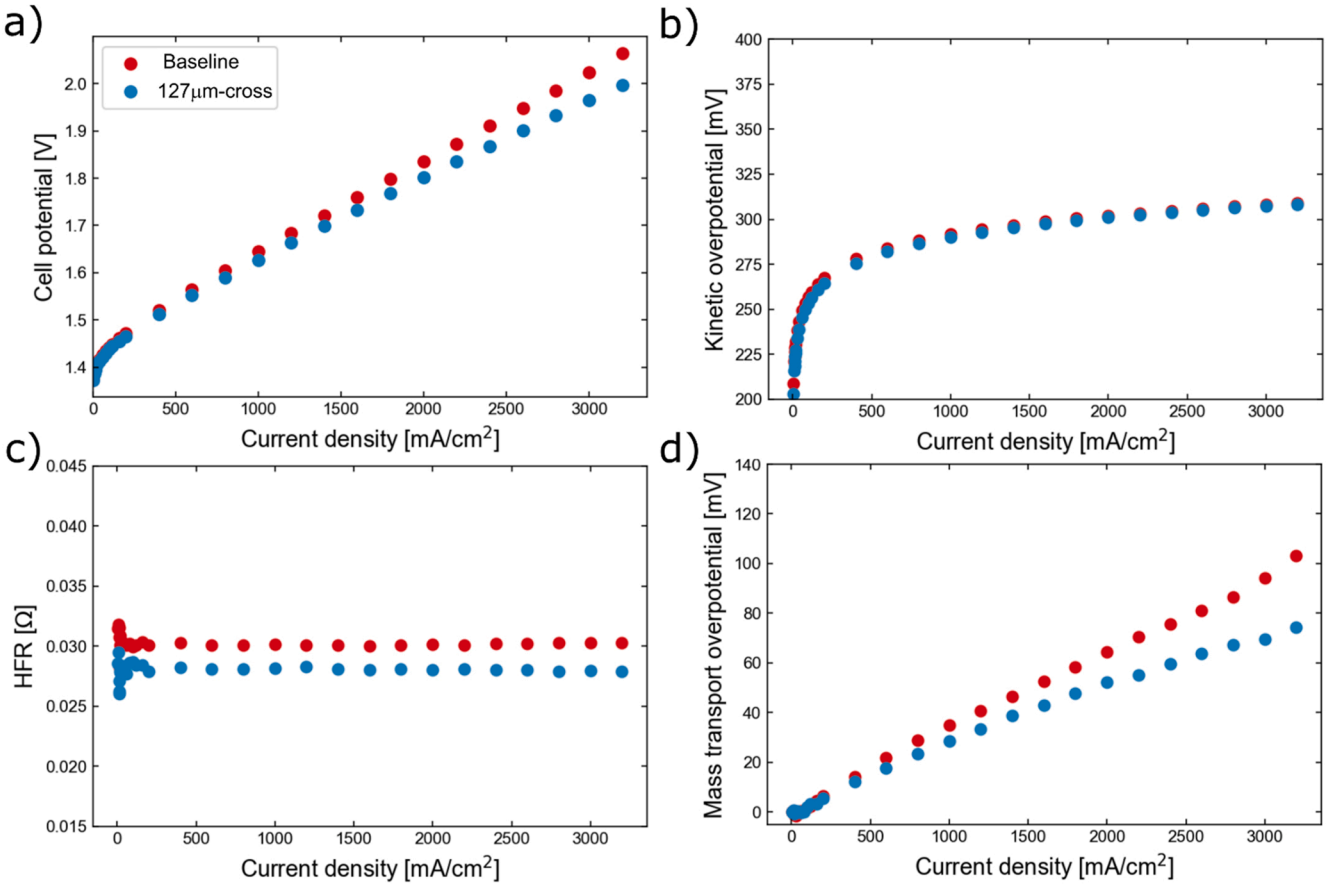

Fig. 8. Applied voltage breakdown of the laser ablated PTL with checker-like structure at high loading (0.4 mg·cm^{-2}). (a) Polarization curve, (b) kinetic overpotential, (c) high frequency resistance and (d) mass transport overpotential in comparison to the baseline PTL. Laser ablated PTL outperforms the baseline PTL at higher loading conditions as well, with improvements in HFR and mass transport losses. The HFR of the laser ablated PTL exhibits similar values at low and high loadings.

observed at ultra-low loadings. Under low catalyst loading conditions, the catalyst layer is significantly thinner and denser than higher catalyst loading conditions. Therefore, mass transport is mostly confined to the two-dimensional space in the through-plane direction, along the pores at the CL-PTL interface. While at relative high catalyst loadings, mass transport is less severe at the interface because thicker catalyst layer

allows gas bubbles transfer to the catalyst layer itself in the three-dimensional space. The gas bubbles generated underneath the flattened titanium phase is then capable of permeating through the pores in the catalyst layer and evacuate through the pores enlarged by the laser ablation. Therefore, effective transport of gas and liquid water develops at the CL-PTL interface on the checker-like structure of laser ablated PTLs. This work demonstrates that laser ablated PTLs enhance electrolyzer performance at both low and high loading conditions without applying a backing layer or an MPL.

2.3. Bulk-phase architecture modification of the porous transport layer

While previous laser ablation focuses on CL-PTL interfacial modifications, this section investigates the strategy of modifying the bulk-phase architecture of PTLs by implementing patternable half-through pore at the flow field-PTL interfaces. Previous studies show that modifying pore structure to enhance mass transport comes at a cost of losing CL-PTL interfacial contact due to the trade-off relationship between interfacial contact and mass transport [15,32]. In fact, some studies highlight that performance lost from the CL-PTL interfacial contact is significantly more harmful to the electrolyzer performance than the improvement obtained from the improved mass transport [28,31,33]. Moreover, some studies demonstrate that these pore structure exacerbate mass transport losses emanated from having poor interfacial contact [28,33]. Therefore, there needs a technique to balance PTL bulk-phase porosity and tortuosity to gain in mass transport and the PTL-CL interfacial contact to enhance electrode kinetics and catalyst utilization. Rationally applying laser-ablation at the flow field-PTL interface to fabricate half-through could help improve the overall PTL porosity and reduce PTL tortuosity while maintaining the PTL-CL interfacial properties.

The electrochemical performance of the patterned half-through pore PTL (on a baseline PTL) and the baseline PTL are shown in Fig. 9. The patterned pore PTL improves the electrolyzer performance by 124 mV at 4 A·cm^{-2}. HFRs and kinetic overpotentials measured from the two PTLs exhibit similar values, with the patterned half-pore PTL performing slightly better. More notable difference in performance of two PTLs comes from the mass transport overpotentials. In particular, the PTL with half-through pores at the flow field interface reduces mass transport overpotentials by 82 mV at 4 A·cm^{-2}. This result reveals that the patterned half-through pore PTL improves mass transport during electrolysis with having minimal impact on the CL-PTL interface. Reduction in the mass transport overpotential will be even more substantial at higher current densities, as demonstrated by Lee et al. and their patterned-through pore PTL, where they improved mass transport overpotential by 76.7% at 9 A·cm^{-2} [26]. Our findings on the half-through pore PTL provide valuable insights for future PTL designs. Fabrication and optimization of patterned half-through pore designs on

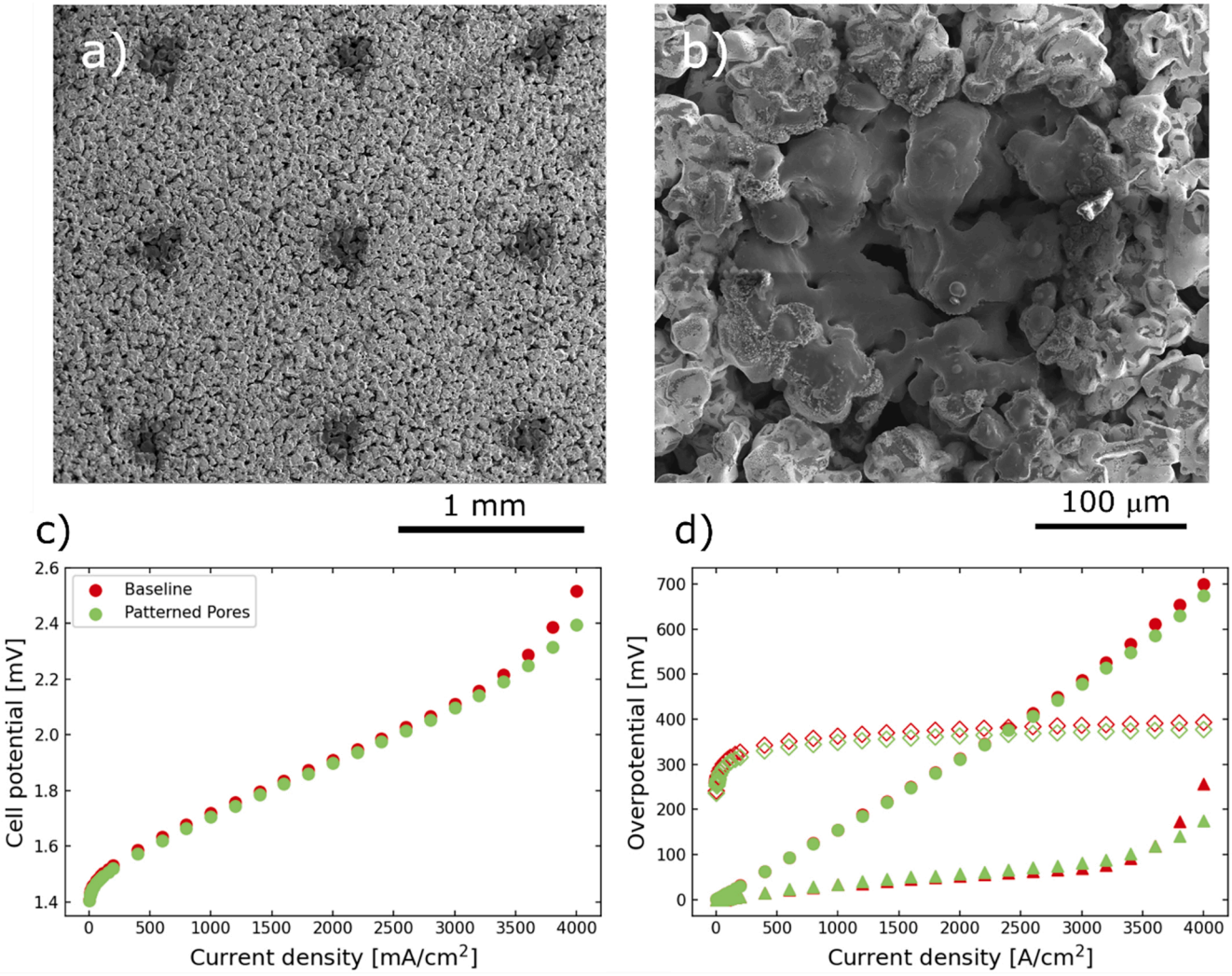

Fig. 9. SEM images of the patterned half-through pore PTL (a and b). Polarization curve (c) and overpotential breakdown (d) of baseline and patterned PTLs under ultra-low loading (0.055 mg·cm^{-2}).

the flow-field interface will enable reduction of mass transport losses without exacerbating losses related to the CL-PTL interface.

3. Conclusion

In this work, we present laser ablation as a facile and scalable technique for modifying the PTL interface to achieve performance improvement of a PEM electrolyzer system. The PTLs are ablated with laser in a parallel pattern and a cross pattern, where the parallel pattern exhibits in land-channel structure and the cross-pattern results in checker-like structure at the CL-PTL interface. The spacing between each laser path is found critical to electrolyzer performance, where shorter spacing is favorable for the parallel pattern while wider spacing is favorable for the cross pattern. Experimental results have shown that the cross-patterned PTL with $d_{path} = 127$ μm exhibited best PTL/CL interface, followed by the parallel-patterned PTL with $d_{path} = 38$ μm. Both patterns outperformed the baseline PTL under both ultra-low (0.055 $mg{\cdot}cm^{-2}$) and high (0.40 $mg{\cdot}cm^{-2}$) loadings. Major improvements are observed from ohmic kinetic overpotentials, where the modified titanium phase provided enlarged contact against the catalyst layer. The CL-PTL interface plays a key role in mass transport under ultra-low loadings because thinner catalyst layer limits transport within the catalyst layer. The best performing laser ablated PTL exhibits reduction of cell potential by 230 mV compared to the baseline PTL under ultra-low loadings. Lastly, we show that bulk modification of the PTL, where fabricating patterned half-through pores at the flow field interface reduced mass transport overpotentials without altering the CL-PTL interface at high current densities. This shows that via laser ablation, optimal PTLs may be designed by ablating both interface as well as the bulk PTL. Our results reveal that laser ablation is a facile and scalable technique for modifying PTL structure to further improve PEM electrolyzer performance under high and ultra-low catalyst loadings.

4. Experimental methods

4.1. Laser ablation of porous transport layers (PTLs)

The surface of the PTL was ablated using a class 4 fiber laser cutter (FIBER50FC, Full Spectrum Laser). Laser power of 5 W at a frequency of 20 kHz was applied to fabricate both patterns (parallel pattern and cross pattern) on the PTL surface. 100 passes were sufficient to modify the morphology of the PTL as shown in Fig. 2. The patterned pore PTL was fabricated by laser ablating 400 pores with a diameter of 200 μm at the PTL-flow field interface. The pores were fabricated in an array of 20 by 20 pores with center-to-center distance being 1 mm. The laser power was set to 5 W at a frequency of 20 kHz and 600 passes were applied. Post to the laser ablation, the PTLs were rinsed first with isopropanol and then with deionized (DI) water. After rinsing, PTLs were submerged in isopropanol for 30 min and underwent chemical etching for 3 min using a commercial Ti metal etchant (Multi-etch). Then, PTLs were coated with Pt to enhance contact properties using a sputtering process. A thin platinum layer was sputtered onto the laser ablated surface of the PTL to provide proficient electrical conductivity. Approximately 40 nm layer of platinum was sputtered onto the laser ablated PTL at a deposition rate of 1.75 Å/s in an Argon environment using AJA RF Sputter System (AJA International Inc.). The deposition rate was obtained by measuring the thickness of the sputtered layer of a sacrificial substrate.

4.2. Preparation of catalyst coated membranes (CCMs):

Ultrasonic spray coating technique was used to prepare CCMs used in this study. The anode ink was made by mixing commercially available iridium oxide (TKK ELC-0110 SA = 100, Tanaka) with water, ethanol, and n-propanol at a ratio of 1:1:2 by volume and adding Nafion ionomer solution (5 wt%, Ion Power D521). The ionomer to iridium ratio was set at 0.116 for all anode catalyst used in this study. Prior to the catalyst deposition, the anode ink was immersed into an ice bath and was sonicated using a horn sonicator (CEX500, Cole-Parmer) at 38% power for 30 min. Information about the anode ink agglomerate size distribution obtained with dynamic light scattering can be seen in Fig. S8. The cathode ink was made by mixing platinum supported by carbon catalyst (TEC10V50E 46.8% Pt, Tanaka) with water and n-propanol at a ratio of 1:1 by volume, and adding Nafion ionomer solution (5 wt%, Ion Power D521). The ionomer to catalyst ratio was set at 0.45 for all cathode catalysts used. The cathode ink was bath sonicated for 30 min at a constant temperature of 10 °C before spray coating. The volume of the ink and ratios were kept identical throughout the study for each loading to ensure minimal impact of ink preparation on electrolyzer performance. 7 thou thick Nafion perfluorosulfonic acid membranes (N117, Ion Power) were used as membrane for fabrication of the CCM. Impurities were removed and protonated the sulfonic-acid groups in Nafion membranes via following processes before spray coating. Membranes were first soaked in DI water at boiling temperature for 1 h and were immersed in 0.5 M HNO_3 (ACS Reagent, Sigma-Aldrich) for 1 h at room temperature. The membranes were then rinsed three times with DI water and were stored in DI water until the spray coating process. The Sono-Tek ultrasonic spray coater was used for catalyst deposition onto the membrane. The sonication was set to 120 kHz, and the membrane was fixed on a vacuum plate at constant temperature of 80 °C to maintain flat surface throughout the spray coating process. X-ray fluorescence (XRF) (Bruker M4 Tornado, Bruker) was used to measure catalyst loadings of both platinum and iridium on the CCM. 0.055 ± 0.005 $mg_{Ir}{\cdot}cm^{-2}$ was targeted for the ultra-low iridium loading and 0.4 ± 0.01 $mg_{Ir}{\cdot}cm^{-2}$ was targeted for high iridium loading. The cathode side platinum was kept constant at 0.1 ± 0.01 $mg_{Pt}{\cdot}cm^{-2}$. The areal dispersion of the ultra-low iridium loading and baseline platinum were as shown in Fig. S7.

4.3. X-ray computed tomography (XCT) and Scanning electron microscope (SEM)

Porous transport layer (PTL) surface morphology was imaged by an FEI Quanta FEG 250 SEM. Ex situ XCT was conducted at the Advanced Light Source at Lawrence Berkeley National Laboratory (Beamline 8.3.2) with a PCO Edge CCD camera, an LuAG scintillator, and 20× optical lenses. The resulting images had a resolution of 0.323 μm voxel−1 and a horizontal field of view of 1.8 mm. The samples were prepared for tomography imaging by cutting the PTLs into ≈3 mm triangular sections each having an ≈45° tip and 5 mm base for mounting on the pins which were mounted on the beamline rotating stage. A multilayer monochromator was used to select the X-ray energy at 20 keV. 300 ms exposure time was used.

4.4. Electrolyzer cell assembly and testing

The active area of CCMs were designed to be 5 cm^2. A single cell hardware (Fuel Cell Technology, FCT) built with platinum coated single channel titanium parallel flow field on the anode and graphite single channel serpentine flow field on the cathode was used for the cell testing. A sintered titanium powder-based PTL (Mott Corp.) was used as a baseline anode PTL and six laser-modified PTLs were used for the study (parallel patterns with $d_{path} = 38$, 76, and 127 μm and cross patterns with $d_{path} = 38$, 76 and 127 μm). 40 nm layer of platinum was sputter coated onto each PTL. A carbon paper without an MPL (Toray 090) was used as the cathode gas diffusion layer (GDL). The thickness of ethylene tetrafluoroethylene (ETFE) gaskets were controlled to achieve 20% compression in the GDL while the thickness of the ETFE gaskets were matched to the titanium PTLs. The electrolyzer cell was applied with a torque of 4.5 Nm to prevent leakage.

A multichannel potentiostat (VSP 300, Biologic) with 20 A booster was used for all electrochemical tests conducted in this study. A modified FCT test station was used for electrolyzer testing. DI water with

recirculation system was fed into the anode of the electrolyzer and fully humidified H_2 was fed into cathode at 80 °C with flow rate of 100 mL·min^{-1}. An auxiliary cell heater was used to heat the cell up to 80 °C. 10 cycles of conditioned cyclic voltammetry measurements (CV) were obtained at a scan rate of 50 mV·s^{-1} between voltage of 1.2 and 2 V prior to measurement of polarization curves and electrochemical impedances. The polarization curve was measured by holding at various constant cell currents for 130 s. Galvanostatic electrochemical impedance spectroscopy was used to measure impedances at each current step. An AC current perturbation between 1 MHz and 100 mHz was applied to the electrolyzer for each current step and measured the following voltage response. The amplitude of the AC current was selected for each step to ensure a sufficient signal to noise ratio while maintaining a linear system response. After measuring polarization curves and impedances, the Ir cyclic voltammetry was measured by cycling from 0.05 to 1.2 V at scanning rate of 50 mV·s^{-1}.

4.5. Applied voltage breakdown

The electrolyzer cell potential, E_{cell}, consists of reversible cell potential, E^0_{rev}, ohmic overpotential, η_{ohmic}, kinetic overpotential, η_{kin}, and mass transport overpotential, η_{mt}:

$$E_{cell} = E^0_{rev} + \eta_{ohmic} + \eta_{kin} + \eta_{mt}$$

We only considered the kinetics and mass transport of the oxygen evolution reaction for this work because oxygen evolution reaction is more sluggish compared to hydrogen evolution reaction. The reversible cell potential was calculated according to the literature [34]:

$$E^0_{rev} = 1.2291 - 0.0008456 \bullet (T - 298.15)$$

where T is temperature [K]. Ohmic overpotential was calculated by measuring high frequency resistance (HFR) during EIS:

$$\eta_{ohmic} = i \bullet HFR$$

where i is the current density [A·cm^{-2}] and HFR is high frequency resistance [Ω·cm^{-2}]. Kinetic overpotential was calculated from Tafel approximation assuming that kinetics are governed by oxygen evolution reaction:

$$\eta_{kin} = b \bullet log\left(\frac{i}{i_0}\right)$$

where b is the measured Tafel slope [V·decade^{-1}] and i_0 is the apparent exchange current density. Finally, mass transport overpotential was calculated by subtracting reversible cell potential, ohmic overpotential and kinetic overpotential from the measured cell potential.

CRediT authorship contribution statement

Jason K. Lee: Conceptualization, Data curation, Formal analysis, Investigation, Methodology, Validation, Visualization, Writing – original draft, Writing – review & editing. **Tobias Schuler:** Investigation, Writing – review & editing. **Guido Bender:** Investigation, Writing – review & editing. **Mayank Sabharwal:** Investigation, Writing – review & editing. **Xiong Peng:** Data curation, Formal analysis, Funding acquisition, Investigation, Methodology, Project administration, Resources, Supervision, Writing – original draft, Writing – review & editing. **Adam Z. Weber:** Data curation, Formal analysis, Funding acquisition, Investigation, Methodology, Project administration, Resources, Supervision, Writing – original draft, Writing – review & editing. **Nemanja Danilovic:** Data curation, Formal analysis, Funding acquisition, Investigation, Methodology, Project administration, Resources, Supervision, Writing – original draft, Writing – review & editing.

Declaration of Competing Interest

The authors declare the following financial interests/personal relationships which may be considered as potential competing interests:

Xiong Peng, Adam Z. Weber, Nemanja Danilovic reports financial support was provided by Fuel Cell Technologies Office. Mayank Sabharwal reports administrative support and equipment, drugs, or supplies were provided by DOE Office of Science User Facility. Nemanja Danilovic, Jason Keonhag Lee, Adam Z Weber, Xiong Peng has patent Laser Ablation of Porous Transport Layers for Water Electrolyzers pending to The Regents of The University of California.

Data availability

Data will be made available on request.

Acknowledgements

The authors acknowledge the Department of Energy–Office of Energy Efficiency and Renewable Energy–Fuel Cell Technologies Office (DOE-EERE-FCTO) and the H_2 from the Next-generation of Electrolyzers of Water (H2NEW) consortium for funding under Contract Number DE-AC02-05CH11231. The micro X-ray CT experiments used beamline 8.3.2 of the Advanced Light Source, which is a DOE Office of Science User Facility under contract no. DE-AC02-05CH11231. We thank Dr. Dula Parkinson for beamline support. All opinions expressed in this paper are the author's and do not necessarily reflect the policies and views of DOE.

Appendix A. Supplementary material

Supplementary data to this article can be found online at https://doi.org/10.1016/j.apenergy.2023.120853.

References

[1] The Future of Hydrogen – Analysis - IEA. https://www.iea.org/reports/the-future-of-hydrogen (accessed 2021-04-19).
[2] Ritchie H, Roser M. CO_2 and greenhouse gas emissions. In: Our world in data; 2020.
[3] Renewable Energy Agency. I. Reaching Zero with Renewables: Eliminating CO2 Emissions from Industry and Transport in Line with the 1.5°C Climate Goal. 2020.
[4] Stöckl F, Schill WP, Zerrahn A. Optimal supply chains and power sector benefits of green hydrogen. Sci Rep 2021;11(1):1–14. https://doi.org/10.1038/s41598-021-92511-6.
[5] Cullen DA, Neyerlin KC, Ahluwalia RK, Mukundan R, More KL, Borup RL, et al. New roads and challenges for fuel cells in heavy-duty transportation. Nat Energy 2021;6(5):462–74. https://doi.org/10.1038/s41560-021-00775-z.
[6] Böhm H, Moser S, Puschnigg S, Zauner A. Power-to-hydrogen & district heating: technology-based and infrastructure-oriented analysis of (future) sector coupling potentials. Int J Hydrogen Energy 2021;46(63):31938–51. https://doi.org/10.1016/J.IJHYDENE.2021.06.233.
[7] Zhang H, Wang L, van Herle J, Maréchal F, Desideri U. Techno-economic comparison of green ammonia production processes. Appl Energy 2020;259:114135. https://doi.org/10.1016/J.APENERGY.2019.114135.
[8] Muslemani H, Liang X, Kaesehage K, Ascui F, Wilson J. Opportunities and challenges for decarbonizing steel production by creating markets for 'green steel' products. J Clean Prod 2021;315:128127. https://doi.org/10.1016/J.JCLEPRO.2021.128127.
[9] Maestre VM, Ortiz A, Ortiz I. Challenges and prospects of renewable hydrogen-based strategies for full decarbonization of stationary power applications. Renew Sustain Energy Rev 2021;152:111628. https://doi.org/10.1016/J.RSER.2021.111628.
[10] Oliveira AM, Beswick RR, Yan Y. A Green hydrogen economy for a renewable energy society. Curr Opin Chem Eng 2021;33:100701. https://doi.org/10.1016/J.COCHE.2021.100701.
[11] Ray; Douglas. Lazard's Levelized Cost of Energy Analysis—Version 13.0. 2020.
[12] Bernt M, Hartig-Weiß A, Tovini MF, El-Sayed HA, Schramm C, Schröter J, et al. Current challenges in catalyst development for PEM water electrolyzers. Chem Ing Tech 2020;92(1–2):31–9. https://doi.org/10.1002/cite.201900101.
[13] Schuler T, de Bruycker R, Schmidt TJ, Büchi FN. Polymer electrolyte water electrolysis: correlating porous transport layer structural properties and performance: part I. tomographic analysis of morphology and topology. J Electrochem Soc 2019;166(4):F270–81. https://doi.org/10.1149/2.0561904jes.
[14] Schuler T, Schmidt TJ, Büchi FN. Polymer electrolyte water electrolysis: correlating performance and porous transport layer structure: part II.

electrochemical performance analysis. J Electrochem Soc 2019;166(10):F555–65. https://doi.org/10.1149/2.1241908jes.
[15] Kim PJ, Lee JK, Lee CH, Fahy KF, Shrestha P, Krause K, et al. Tailoring catalyst layer interface with titanium mesh porous transport layers. Electrochim Acta 2021; 373:137879. https://doi.org/10.1016/J.ELECTACTA.2021.137879.
[16] Parra-Restrepo J, Bligny R, Dillet J, Didierjean S, Stemmelen D, Moyne C, et al. Influence of the porous transport layer properties on the mass and charge transfer in a segmented PEM electrolyzer. Int J Hydrogen Energy 2020;45(15):8094–106. https://doi.org/10.1016/j.ijhydene.2020.01.100.
[17] Taie Z, Peng X, Kulkarni D, Zenyuk IV, Weber AZ, Hagen C, et al. Pathway to complete energy sector decarbonization with available iridium resources using ultralow loaded water electrolyzers. ACS Appl Mater Interfaces 2020;12(47): 52701–12. https://doi.org/10.1021/acsami.0c15687.
[18] Lettenmeier P, Kolb S, Burggraf F, Gago AS, Friedrich KA. Towards developing a backing layer for proton exchange membrane electrolyzers. J Power Sources 2016; 311:153–8. https://doi.org/10.1016/j.jpowsour.2016.01.100.
[19] Lettenmeier P, Kolb S, Sata N, Fallisch A, Zielke L, Thiele S, et al. Energy & environmental science comprehensive investigation of novel pore-graded gas diffusion layers for high-performance and cost-effective proton exchange membrane electrolyzers †. Energ Environ Sci 2017;10:2521. https://doi.org/10.1039/c7ee01240c.
[20] Stiber S, Sata N, Morawietz T, Ansar SA, Jahnke T, Lee JK, et al. A high-performance, durable and low-cost proton exchange membrane electrolyser with stainless steel components. Energ Environ Sci 2022;15(1):109–22. https://doi.org/10.1039/D1EE02112E.
[21] Stiber S, Balzer H, Wierhake A, Wirkert FJ, Roth J, Rost U, et al. Porous transport layers for proton exchange membrane electrolysis under extreme conditions of current density, temperature, and pressure. Adv Energy Mater 2021;11(33): 2100630. https://doi.org/10.1002/AENM.202100630.
[22] Schuler T, Ciccone JM, Krentscher B, Marone F, Peter C, Schmidt TJ, et al. Hierarchically structured porous transport layers for polymer electrolyte water electrolysis. Adv Energy Mater 2020;10(2):1903216. https://doi.org/10.1002/aenm.201903216.
[23] Mo J, Kang Z, Yang G, Retterer ST, Cullen DA, Toops TJ, et al. Thin liquid/gas diffusion layers for high-efficiency hydrogen production from water splitting. Appl Energy 2016;177:817–22. https://doi.org/10.1016/j.apenergy.2016.05.154.
[24] Mo J, Kang Z, Retterer ST, Cullen DA, Toops TJ, Green JB, et al. Discovery of true electrochemical reactions for ultrahigh catalyst mass activity in water splitting. Sci Adv 2016;2(11). https://doi.org/10.1126/sciadv.1600690.
[25] Kang Z, Mo J, Yang G, Retterer ST, Cullen DA, Toops TJ, et al. Investigation of thin/well-tunable liquid/gas diffusion layers exhibiting superior multifunctional performance in low-temperature electrolytic water splitting. Energ Environ Sci 2017;10(1):166–75. https://doi.org/10.1039/c6ee02368a.
[26] Bazylak A, Lee JK, Lee CH, Fahy KF, Kim PJ, Krause K, et al. Accelerating bubble detachment in porous transport layers with patterned through-pores. ACS Appl Energy Mater 2020;3(10):9676–84. https://doi.org/10.1021/acsaem.0c01239.
[27] Suermann M, Gimpel T, Bühre LV, Schade W, Bensmann B, Hanke-Rauschenbach R. Femtosecond laser-induced surface structuring of the porous transport layers in proton exchange membrane water electrolysis. J Mater Chem A 2020. https://doi.org/10.1039/C9TA12127G.
[28] Majasan JO, Iacoviello F, Shearing PR, Brett DJL. Effect of microstructure of porous transport layer on performance in polymer electrolyte membrane water electrolyser. Energy Procedia 2018;151:111–9. https://doi.org/10.1016/j.egypro.2018.09.035.
[29] Lee JK, Lee CH, Bazylak A. Pore network modelling to enhance liquid water transport through porous transport layers for polymer electrolyte membrane electrolyzers. J Power Sources 2019;437:226910. https://doi.org/10.1016/j.jpowsour.2019.226910.
[30] Peng X, Satjaritanun P, Taie Z, Wiles L, Keane A, Capuano C, et al. Insights into interfacial and bulk transport phenomena affecting proton exchange membrane water electrolyzer performance at ultra-low iridium loadings. Adv Sci 2021;8(21). https://doi.org/10.1002/ADVS.202102950.
[31] Parra-Restrepo J, Bligny R, Dillet J, Didierjean S, Stemmelen D, Moyne C, et al. Influence of the porous transport layer properties on the mass and charge transfer in a segmented PEM electrolyzer. Int J Hydrogen Energy 2020. https://doi.org/10.1016/j.ijhydene.2020.01.100.
[32] Lee JK, Bazylak A. Optimizing porous transport layer design parameters via stochastic pore network modelling: reactant transport and interfacial contact considerations. J Electrochem Soc 2020;167(1):013541. https://doi.org/10.1149/1945-7111/ab6557.
[33] Lopata J, Kang Z, Young J, Bender G, Weidner JW, Shimpalee S. Effects of the transport/catalyst layer Interface and catalyst loading on mass and charge transport phenomena in polymer electrolyte membrane water electrolysis devices. J Electrochem Soc 2020;167(6):064507. https://doi.org/10.1149/1945-7111/ab7f87.
[34] Bratsch SG. Standard electrode potentials and temperature coefficients in water at 298.15 K. J Phys Chem Ref Data Monogr 2009;18(1):1. https://doi.org/10.1063/1.555839.